A Statistical Forecast Model of Tropical Intraseasonal Convective Anomalies

CHARLES JONES

Institute for Computational Earth System Science, University of California, Santa Barbara, Santa Barbara, California

LEILA M. V. CARVALHO

Department of Atmospheric Sciences, Institute of Astronomy, Geophysics and Atmospheric Sciences, University of São Paulo, São Paulo, Brazil

R. WAYNE HIGGINS

NOAA/NWS/NCEP Climate Prediction Center, Washington, D.C.

DUANE E. WALISER

Institute for Terrestrial and Planetary Atmospheres, State University of New York at Stony Brook, Stony Brook, New York

J.-K. E. SCHEMM

NOAA/NWS/NCEP Climate Prediction Center, Washington, D.C.

(Manuscript received 21 November 2002, in final form 28 November 2003)

ABSTRACT

Tropical intraseasonal convective anomalies (TICAs) play a significant role in the coupled ocean–atmosphere system and the Madden–Julian oscillation (MJO) is the primary mode of this variability. This study describes statistical forecast models of intraseasonal variations. Twenty-four years of outgoing longwave radiation (OLR) and zonal components of the wind at 200 (U200) and 850 hPa (U850) are used. The models use the principal components (PCs) of combined EOF analysis of 20–90-day anomalies of OLR, U200, and U850 data. Forecast models are developed for each lead time from 1 to 10 pentads and for winter and summer seasons separately. The forecast models use a combination of the five most recent pentad values of the first five PCs of the combined EOF of (OLR, U200, U850) to predict the future values of a given PC_k ($k = 1, 5$). The spatial structures are obtained by reconstructing the fields of OLR, U200, and U850 using the forecasts of PC_k ($k = 1, 5$) and the associated EOFs. Verification with independent winter and summer data indicates useful forecasts of the first five PCs extending up to five pentads of lead time. The verification against 20–90-day anomalies indicates useful forecasts of the reconstructed fields of OLR, U200, and U850 extending up to four pentads of lead time over most of the Tropics. Furthermore, the statistical models provide useful forecasts of U200 and U850 intraseasonal anomalies up to two to three pentads of lead times in portions of the North Pacific region.

1. Introduction

Several studies have demonstrated that intraseasonal variations in tropical convective activity (roughly 10–90 days) represent an important forcing mechanism in the atmosphere (e.g., Rasmusson and Arkin 1993; Salby and Hendon 1994). A recent climatology of tropical intraseasonal convective anomalies has been discussed in Jones et al. (2004a). On this time scale, the Madden–Julian oscillation (MJO) is the dominant mode of tropical intraseasonal variability (Madden and Julian 1994). The MJO influences the precipitation patterns associated with the monsoons in Asia, Australia, North America, and South America (Yasunari 1979; Lau and Chan 1986; Mo 2000; Higgins and Shi 2001; Jones and Carvalho 2002). This influence has also been shown to modulate rainfall variability and extreme events in the Americas (Higgins et al. 2000; Jones 2000; Nogués-Paegle et al. 2000; Whitaker and Weickmann 2001; Carvalho et al. 2004). Furthermore, the eastward propagation of MJO events over the equatorial Pacific Ocean significantly modifies the thermocline structure via their connection to westerly wind bursts (e.g., McPhaden 2002). Although the MJO does not cause El Niño–Southern Oscillation (ENSO), the MJO contributes to its rate of

Corresponding author address: Dr. Charles Jones, Institute for Computational Earth System Science, University of California, Santa Barbara, Santa Barbara, CA 93106.
E-mail: cjones@icess.ucsb.edu

development and (possibly) its ultimate intensity through the generation of eastward-propagating oceanic Kelvin waves (McPhaden 2002; Kessler 2001).

The influential nature of the MJO has also been noted on medium-to-extended-range numerical weather forecasts. Ferranti et al. (1990), for instance, demonstrated that forecast skills in the extratropics are significantly improved when the errors associated with the representation of the tropical intraseasonal oscillation are minimized. Jones et al. (2004b) conducted predictability experiments to show that the MJO influences the Northern Hemisphere weather predictability. However, a major difficulty to evaluate the predictive skill of the MJO and its impacts on medium-to-extended-range forecasts relates to the inability that most numerical models have to realistically represent the MJO (Lau and Chang 1992; Hendon et al. 2000; Jones et al. 2000; Jones and Schemm 2000). Currently, useful forecast skills of the MJO from operational numerical models extend to only about 7–10 days.

Motivated by the facts mentioned above, a few studies have developed statistical techniques to estimate the predictive skill of the MJO. Waliser et al. (1999) used 18 yr of bandpassed (30–70 days) outgoing longwave radiation (OLR) data and a statistical model based on singular value decomposition. The model uses the two most recent pentad maps of bandpassed OLR anomalies as predictors and predicts the evolution of intraseasonal OLR anomalies. In general, winter and summer season validation against bandpassed anomalies indicates useful skills out to 5–20 days over most of the Eastern Hemisphere. Lo and Hendon (2000) used a lag regression model that uses as predictors the first two and first three principal components of spatially filtered OLR and streamfunction, respectively. The statistical model, which was developed only for the boreal winter season, indicates skillful forecasts out to 15 days of lead time. Similarly, a combination of singular spectral analysis and maximum entropy method employed by Mo (2001) indicates correlation skills of 0.65 at lead times of four pentads. Wheeler and Weickmann (2001) developed a tropical wave theory filtering technique to forecast tropical convectively coupled modes as determined by OLR variability. In their model, useful statistical forecast skill of the MJO was also in the range of 15–20 days. Thus, despite differences in methodological approach, the forecast skill of the MJO obtained with statistical models is generally on the order of 15–20 days of lead time.

Recently, there has been an increasing interest in exploiting the predictability of weather and short-term climate variability on subseasonal time scales, that is, beyond two weeks but shorter than about two months (Schubert et al. 2002). In this context, the MJO plays an important role given its influence on weather and climate variability in the Tropics as well as extratropics. Therefore, the objective of this paper is to contribute to this research effort by describing a statistical forecast model of tropical intraseasonal convective anomalies (TICAs). Datasets are described in section 2. The model construction and validation with independent data are presented in section 3. The evaluation of forecast skill during winter and summer seasons are discussed in section 4. Section 5 summarizes the results and conclusions.

2. Data

Outgoing longwave radiation is employed as a proxy for large-scale tropical convective activity (e.g., Lau and Chan 1986; Jones et al. 1998). Pentads of OLR (5-day nonoverlapping averages; 73 pentads yr^{-1}) were used from 1–5 January 1979 to 27–31 December 2002 (1752 pentads). Additional information on changes in instrumentation, equator-crossing times, and inherent biases in the OLR data are described in Chelliah and Arkin (1992) and Lucas et al. (2001). The large-scale circulation is described with pentads of the zonal components of the wind at 200 (U200) and 850 hPa (U850) obtained from the National Centers for Environmental Prediction–National Center for Atmospheric Research (NCEP–NCAR) reanalysis (Kalnay et al. 1996). The spatial resolutions of the OLR, U200, and U850 fields were decreased to 5° × 5° latitude–longitude to focus on large-scale features of TICA characteristics, and the domain of analysis extends from 60°S to 60°N and all longitudes (1728 points in space).

The time series of OLR, U200, and U850 were filtered in frequency domain with fast Fourier transform (FFT) and only periods between 20 and 90 days were retained. The OLR anomalies were additionally filtered in space with a weighted average spatial filter such that each filtered value is given by $\mathrm{OLR}'_j = 0.5 \times \mathrm{OLR}_j + \sum_{k=1}^{8} 1/8 \times \mathrm{OLR}_k$, where the summation is for the eight neighbor points of OLR_j.

3. Model construction

In this section, we describe in detail the steps involved in the construction of the statistical forecast model. The datasets of bandpassed-filtered OLR, U200, and U850 were first separated in two parts each with 876 pentads, such that the period from 1–5 January 1979 to 27–31 December 1990 was used for model development and the period from 1–5 January 1991 to 27–31 December 2002 for model validation. The results were insensitive if the developing and validation samples were inverted.

a. Empirical orthogonal function analysis

To begin with, we discuss the results of empirical orthogonal function (EOF) analysis (Kutzbach 1967), because it forms the basis of our statistical forecast model. The EOF analysis was performed on the development and validation samples separately. The results for the validation sample (876 pentads) are discussed in this section and they were computed for each field separately

TABLE 1. Percentage of explained variance of the first 10 eigenvalues of EOF analysis of OLR, U200, U850 and combined EOF (OLR, U20, U850). Sampling errors are indicated in parentheses.

	Percentage of explained variance (sampling error)			
Mode	OLR	U200	U850	(OLR, U200, U850)
1	7.18 (0.77)	5.13 (0.55)	4.63 (0.50)	5.13 (0.55)
2	5.79 (0,62)	4.65 (0.50)	4.47 (0.48)	4.30 (0.46)
3	3.43 (0.37)	3.61 (0.39)	4.08 (0.44)	2.46 (0.26)
4	2.76 (0.29)	3.38 (0.36)	3.92 (0.42)	2.13 (0.23)
5	2.54 (0.27)	3.07 (0.33)	3.63 (0.39)	2.03 (0.22)
6	2.27 (0.24)	2.91 (0.31)	3.45 (0.37)	1.84 (0.20)
7	2.01 (0.21)	2.77 (0.30)	2.96 (0.32)	1.79 (0.19)
8	1.78 (0.19)	2.57 (0.28)	2.90 (0.31)	1.62 (0.17)
9	1.75 (0.19)	2.21 (0.24)	2.72 (0.29)	1.56 (0.17)
10	1.71 (0.18)	2.15 (0.23)	2.42 (0.26)	1.49 (0.16)
	31.22	32.46	35.19	24.34

as well as for them combined (OLR, U200, U850). The selection of the spatial domain (60°S–60°N; all longitudes) is motivated by our intent to develop a statistical forecast model that captures the covariability of tropical intraseasonal convective anomalies and extratropical large-scale circulation (see also section 5). Prior to EOF calculation, each grid point of each field was scaled by the square root of the cosine of the latitude.

The EOF computation for a single field involves a data matrix A with dimensions 876 pentads by 1728 points in space. Likewise, the combined EOF of (OLR, U200, U850) has dimensions of 876 pentads by 5184 points in space (three parameters $\times$ 1728). Because the number of points in space is significantly larger than in time, the eigenvector calculation was done on the correlation matrix $\mathbf{C}$ with dimensions 876 $\times$ 876. This alternate method of EOF computation (Hirose and Kutzbach 1969) is computationally efficient, and it ensures that the estimated eigenvalues are stable (Preisendorfer 1988).

Table 1 shows the percentage of total intraseasonal variance explained by the first 10 eigenvalues computed for each field separately as well as for them combined (OLR, U200, U850). The sampling error computed according to North et al. (1982) and assuming independent events every 10 pentads is also shown. Many previous studies have shown that the first two EOFs capture the propagating behavior of the MJO (Jones 2000; Lo and Hendon 2000). In a recent study, Kessler (2001) pointed out that some of the ENSO effect on the MJO is captured by the third EOF. Together, the first three eigenvalues account for 16.4%, 13.4%, 13.2%, and 11.9% of the OLR, U200, U850, and (OLR, U200, U850) calculations, respectively. In addition, there are not large differences in the percentages of variance explained by the first three eigenvalues for the different EOF analysis. The cumulative percentages of total variance explained by the first 10 eigenvalues are also indicated.

Figure 1 shows the spatial variability corresponding to the first combined EOF (OLR, U200, U850). When there is enhanced convective activity in the equatorial Indian Ocean (top panel), easterlies and westerlies are observed in the zonal wind component at 200 hPa (middle panel). Likewise, enhanced westerly and easterly anomalies are observed in the zonal wind component at 850 hPa (bottom panel). The second EOF pattern (Fig. 2) shows enhanced convection over Indonesia (top panel) and the corresponding westerly and easterly relationships in U200 (middle panel) and U850 anomalies (bottom panel). Figure 3 displays the spatial variability of intraseasonal anomalies of OLR, U200, and U850 associated with the third combined EOF.

As explained before, the combined EOF was computed from the correlation matrix of OLR, U200, U850 data. An alternative procedure is to normalize each field separately and then compute the covariance matrix and EOFs. Although the results are similar, the former procedure results in more coherent spatial patterns that are smoother than the latter method. Thus, the combined EOF calculation from the correlation matrix was adopted.

The principal components (PCs) associated with the combined EOF describe the time variability (not shown). As it will be explained later, using the combined EOF (OLR, U200, U850) to construct the forecast models provides slightly better results than the ones based on the EOF of OLR by itself. In addition, the statistical model based on the combined EOF has the advantage of providing forecasts of all three fields together. Thus, in the remainder of this paper we consider the two sets of PCs and the spatial patterns of the combined EOF (OLR, U200, U850) derived from the development and validation samples separately.

b. Winter forecast models

The statistical forecast models were developed for winter and summer seasons separately. The development (validation) sample was divided into 11 extended winter seasons (from 17–21 November to 11–15 May) 1979/80–1989/90 (1991/92–2001/02). Our approach to construct the statistical forecast models relies on the ''memory'' (i.e., autocorrelation) contained in the PCs derived from the combined EOF as well as the lag correlations among the PCs. We start the discussion by showing the sensitivity tests performed and finally discussing the selected model.

The first step is to determine the appropriate model order based on autoregressive processes. An autoregressive (AR) model of order m can be written as

AR(m):

$$\mathrm{PC}_K(t+1) = \sum_{j=1}^{m} \phi_j \mathrm{PC}_K(t-j+1) + \varepsilon_{t+1}, \quad (1)$$

where the left-hand side is the future value of the principal component PC_K, ϕ_j are the autoregressive parameters determined by the Yule–Walker equations and ε_{t+1} is a random component (Wilks 1995). The order selec-

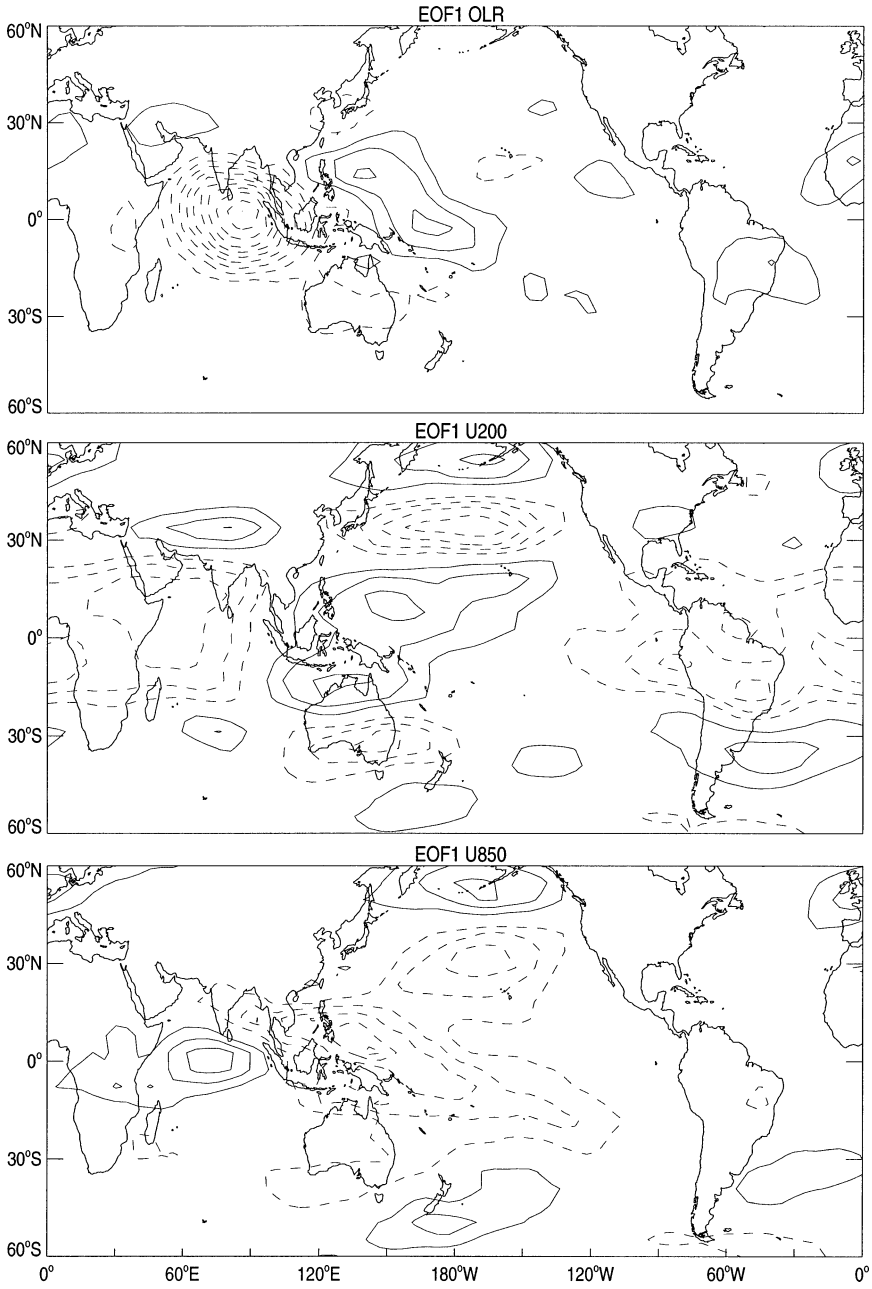

FIG. 1. First eigenvectors of combined EOF analysis of (top) OLR-, (middle) U200-, and (bottom) U850-filtered (20–90 day) anomalies. Solid (dashed) contours indicate positive (negative) values in arbitrary units. Contouring interval is 50.

tion of the AR model is important so that overfitting is avoided. This question can be examined by computing the Bayesian information criterion (BIC) and Akaike information criterion (AIC) statistics given by

$$\mathrm{BIC}(m) = n \ln\left[\frac{n}{n-m-1} S_\varepsilon^2(m)\right] + (m+1)\ln(n) \quad (2)$$

$$\mathrm{AIC}(m) = n \ln\left[\frac{n}{n-m-1} S_\varepsilon^2(m)\right] + 2(m+1), \quad (3)$$

where n is the sample size and $S_\varepsilon^2(m)$ is the sample white noise variance estimated with the recursive equation proposed by Katz (1982):

$$S_\varepsilon^2(m) = [1 - \phi_m^2(m)]S_\varepsilon^2(m-1). \quad (4)$$

Note that $S_\varepsilon^2(0)$ is the variance of the PC_K series. The BIC and AIC statistics involve log-likelihood and a penalty for the number of parameters. The better fitting models exhibit less uncertainty in the residual variance

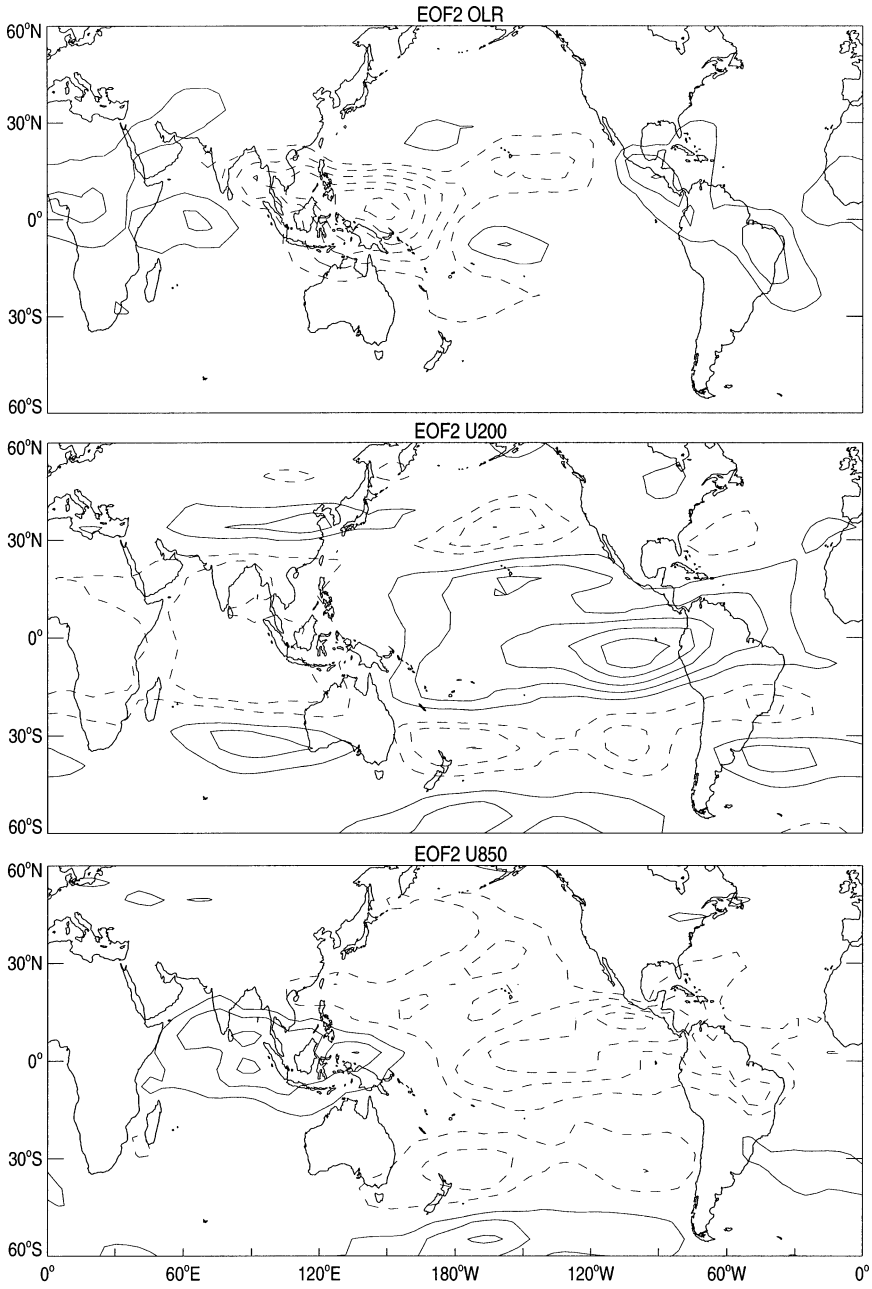

FIG. 2. Second eigenvectors of combined EOF analysis of (top) OLR-, (middle) U200-, and (bottom) U850-filtered (20–90 day) anomalies. Solid (dashed) contours indicate positive (negative) values in arbitrary units. Contouring interval is 50.

and smaller white noise variance. The reader is referred to Wilks (1995; 302–314) for further details.

The AR models were fitted to the first 10 PCs (k = 1, 10) and the order of the models varied from m = 1, 10. Stationarity for all models were tested following the approach of Jenkins and Watts (1968). For simplicity, Table 2 summarizes the results for the first five PCs and the first six AR models. Both BIC and AIC statistics systematically indicate that AR(5) minimizes the white noise residual variance for PC_K, K = 1, 5. Thus, these results suggest that using the five most recent values of the PCs can provide efficient and stable AR models.

The second test consisted in developing forecast models such that the future values of a given PC_K are determined by multiple linear regressions of the previous values of a pair of PCs, that is,

$$PC_K(t + \tau) = \sum_{j=1}^{\lambda} \sum_{p=1}^{m} B_{pj}(\tau) PC_p(t - j + 1). \quad (5)$$

Note that there is one forecast model for each lead

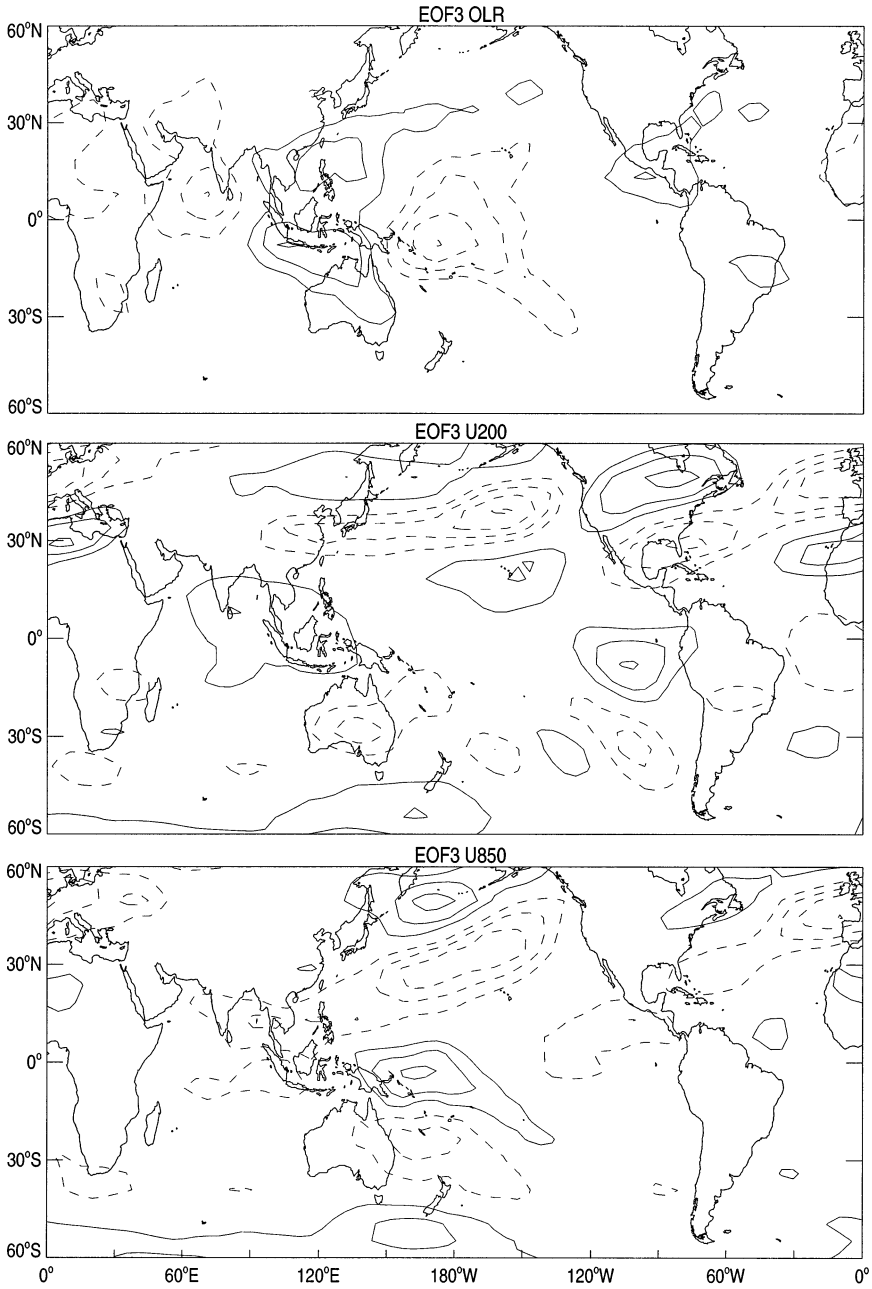

FIG. 3. Third eigenvectors of combined EOF analysis of (top) OLR-, (middle) U200-, and (bottom) U850-filtered (20–90 day) anomalies. Solid (dashed) contours indicate positive (negative) values in arbitrary units. Contouring interval is 50.

time τ, which is computed for $\tau = 1, 10$ pentads. In this experiment, we are concerned with testing the sensitivity to increasing the lag λ. To illustrate this, we show the results for the first two PCs of the combined EOF (OLR, U200, U850), because the results were similar for all 10 PCs. Thus, in this case, $k = m = 1, 2$ and λ varied from 1 to 6 for the most recent pentads. The multiple linear regressions were determined from the developing sample.

Figure 4 shows the forecast skill of the different PC1 and PC2 models using the validation sample. The correlations for PC1 models (Fig. 4a) show that there is a large improvement when λ is greater than two pentads. In particular, for $\lambda = 5$ pentads, the correlation is slightly above 0.5 at five pentads of lead time. Another way of evaluating the forecast skill is by computing standardized root-mean-square error (rmse) (Fig. 4c). The forecasts models using $\lambda \geq 4$ pentads have smaller error growth than models $\lambda \leq 3$ pentads and reach a value of rms $= 1$ by about five pentads of lead time. Similar

TABLE 2. Winter results from AR models fitted to the first five PCs of combined EO analysis (OLR, U200, U850). Lag, m indicates the order of the AR model, R_m is the mth lag autocorrelation, $S^2_\epsilon(m)$ is the white noise residual variance, and BIC and AIC are the statistics used to evaluate the best order of the AR $E - m = \times 10^{-n}$ model. Bold values indicate local minimum.

	Winter AR models				
	Lag, m	R_m	$S^2_\epsilon(m)$	BIC	AIC
PC1	**0**	1.00	1.219E-03	−2643.0	−2651.0
	1	0.71	5.998E-04	−2923.9	−2931.9
	2	0.13	2.315E-04	−3293.9	−3305.8
	3	−0.35	2.157E-04	−3314.9	−3330.9
	4	−0.53	1.847E-04	−3369.4	−3389.3
	5	−0.52	1.710E-04	**−3393.0**	**−3416.9**
	6	−0.39	1.709E-04	−3386.2	−3414.1
PC2	**0**	1.00	1.467E-03	−2569.9	−2577.9
	1	0.72	7.073E-04	−2858.6	−2866.6
	2	0.14	2.725E-04	−3229.4	−3241.4
	3	−0.33	2.586E-04	−3243.0	−3259.0
	4	−0.54	2.267E-04	−3288.2	−33.08.1
	5	−0.53	2.137E-04	**−3304.6**	**−3328.5**
	6	−0.39	2.137E-04	−3297.7	−3325.6
PC3	**0**	1.00	1.272E-03	−2626.3	−2634.3
	1	0.65	7.328E-04	−2844.6	−2852.6
	2	0.02	3.726E-04	−3105.5	−3117.5
	3	−0.36	3.478E-04	−3125.8	−3141.7
	4	−0.38	3.248E-04	−3145.8	−3165.7
	5	−0.29	3.030E-04	**−3166.4**	**−3190.3**
	6	−0.24	3.018E-04	−3160.9	−3188.8
PC4	**0**	1.00	1.182E-03	−2655.3	−2663.3
	1	0.71	5.913E-04	−2929.6	−2937.6
	2	0.15	2.989E-04	−3192.8	−3204.7
	3	−0.23	2.688E-04	−3227.8	−3243.8
	4	−0.35	2.364E-04	−3271.6	−3291.5
	5	−0.39	2.104E-04	**−3310.8**	**−3334.7**
	6	−0.42	2.104E-04	−3303.8	−3331.7
PC5	**0**	1.00	1.122E-03	−2675.9	−2683.8
	1	0.59	7.299E-04	−2846.2	−2854.2
	2	−0.13	3.338E-04	−3149.0	−3161.0
	3	−0.47	2.983E-04	−3186.5	−3202.4
	4	−0.36	2.573E-04	−3238.1	−3258.0
	5	−0.18	2.448E-04	**−3250.8**	**−3274.7**
	6	−0.1128	2.448E-04	−3243.8	−3271.7

behavior is observed for the validation of forecast models for PC2 (Figs. 4b,d). Increasing $\lambda > 6$ pentads brings little improvement. These results suggest that forecasts models based on PCs that use the five most recent pentads can provide useful forecasts of the MJO. The choice of $\lambda = 5$ pentads is consistent with the results of the AR models described before. It is also interesting that $\lambda = 5$ pentads is about half of the life cycle of the MJO.

The third test performed was intended to evaluate how much skill is gained by increasing the number of PCs as predictors in the multiple linear regressions. In order to address this issue, we fixed $\lambda = 1$ pentad and increased the number of PCs as predictors:

$$\mathrm{PC}_K(t + \tau) = \sum_{p=1}^{m} B_p(\tau)\mathrm{PC}_p(t - 1). \quad (6)$$

In this experiment, we varied $K = 1$, 10 and $m = 1$, 10. To make the presentation more manageable, we show the results for $K = 1$, 2 and $m = 1$, 10. The regression parameters were determined from the developing sample and Table 3 shows the forecast verification obtained with the validation sample.

In contrast to increasing the lag λ, increasing the number of PCs as predictors does not show obvious results, although some tendencies are perceptible. For instance, the correlation for PC1 forecast using only PC1 as predictor is 0.72 at one pentad of lead time (Table 3, first row). Increasing the number of PCs increases the skill only to about four or five PCs, then there seems to be a decrease in the forecast skill. The same comment can be made for the PC2 verification. After collectively analyzing the results for PC_K, $k = 1$, 5, it was concluded that increasing the number of PCs to $m = 5$ brings some modest improvement in the forecast skill.

Based on the sensitivity tests described before, the following forecast models are proposed:

$$\mathrm{PC}_K(t + \tau) = \sum_{p=1}^{m} \sum_{j=1}^{\lambda} B_{pj}(\tau)\mathrm{PC}_p(t - j + 1). \quad (7)$$

For each PC_K, $k = 1$, 5 and each lead time $\tau = 1$, 10 pentads, there are 25 predictors such that $m = 1$, 5 and $\lambda = 1$, 5 pentads. The regression parameters for the selected models were determined from the developing sample and Fig. 5 shows the skill for the validation sample. Except for PC4, forecast skills of all PCs extend to about five pentads of lead time both in terms of correlation and standardized rms errors. The superior forecast skill relative to persistence is quite clear (Fig. 5 top, dashed line). In summary, our selected forecast models use a combination of the five most recent pentad values of the first five PCs of the combined EOF (OLR, U200, U850) of intraseasonal anomalies to predict the future values of a given PC_K ($k = 1$, 5).

c. Summer forecast models

The analysis for the construction of forecast models for the summer season was developed in a similar manner. The development (validation) sample was divided into 12 extended summer seasons (from 16–20 May to 12–16 November) 1979–90 (1991–2002). For completeness, we show the same sensitivity tests described before. Table 4 displays the AR models, BIC and AIC statistics. Coincidently, the BIC and AIC statistics also indicate that using AR models of order $m = 5$ minimize the residual white noise variance.

The experiment to test the sensitivity to increasing lags λ [Eq. (5)] is displayed in Fig. 6, which was computed for the validation sample. Quite similar results to the winter case are observed, and indicate that using the five most recent pentad values produce useful forecast skills up to about five pentads of lead time measured with both correlations and standardized rms errors. Note that relative to the winter case, forecast models for PC2 seem to exhibit slightly more skill (about six pentads).

Table 5 shows the results to test the sensitivity to

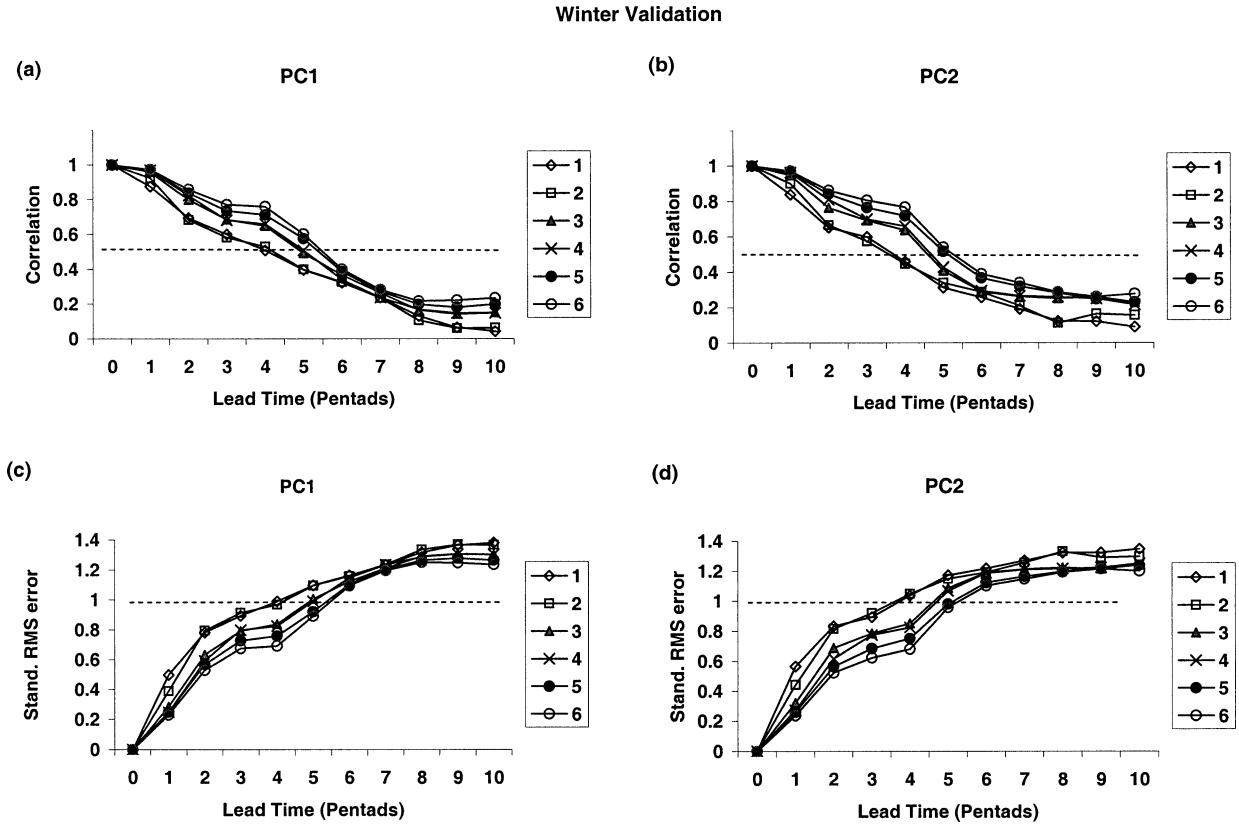

FIG. 4. Winter sensitivity test to increasing lags of PC predictors [see Eq. (5)]. (a), (b) Correlations between forecasts and validation values of PC1 and PC2. Each curve indicates the lag (one to six pentads). (c), (d) Standardized rms errors between forecasts and validation values of PC1 and PC2. Verification is performed on 11 winter seasons of independent data.

TABLE 3. Winter forecast validations of (top) PC1 and (bottom) PC2. Lead times (pentads) are indicated in the leftmost vertical column. The number of PCs used as predictors are indicated in the first horizontal line (1–10) [see Eq. (7) and text for details]. Values indicate correlations between forecast and validation.

Winter validation—PC1 correlation										
Lead	1	2	3	4	5	6	7	8	9	10
1	0.72	0.88	0.88	0.88	0.87	0.86	0.86	0.86	0.85	0.85
2	0.10	0.69	0.69	0.69	0.68	0.65	0.66	0.67	0.55	0.55
3	0.37	0.60	0.60	0.58	0.58	0.58	0.59	0.59	0.53	0.53
4	0.50	0.51	0.48	0.50	0.51	0.50	0.50	0.50	0.50	0.50
5	0.41	0.40	0.33	0.33	0.33	0.33	0.33	0.33	0.32	0.32
6	0.28	0.32	0.28	0.24	0.23	0.24	0.24	0.26	0.23	0.24
7	0.15	0.24	0.24	0.22	0.23	0.21	0.21	0.25	0.21	0.20
8	−0.04	0.13	0.12	0.12	0.14	0.12	0.13	0.15	0.15	0.14
9	0.02	0.07	0.07	0.07	0.07	0.09	0.11	0.12	0.14	0.16
10	0.03	0.04	0.03	0.04	0.04	0.05	0.05	0.05	0.08	0.10
Winter validation—PC2 correlation										
Lead	1	2	3	4	5	6	7	8	9	10
1	0.57	0.84	0.84	0.84	0.83	0.84	0.81	0.81	0.81	0.80
2	0.66	0.65	0.64	0.65	0.65	0.67	0.65	0.64	0.63	0.63
3	0.42	0.60	0.58	0.58	0.57	0.58	0.58	0.58	0.58	0.58
4	0.11	0.46	0.44	0.43	0.43	0.42	0.42	0.44	0.39	0.39
5	0.08	0.31	0.31	0.30	0.31	0.30	0.30	0.32	0.29	0.29
6	0.16	0.26	0.21	0.21	0.20	0.18	0.19	0.19	0.19	0.19
7	0.16	0.19	0.09	0.09	0.08	0.08	0.08	0.09	0.13	0.14
8	0.12	0.12	0.04	0.04	0.04	0.06	0.06	0.05	0.11	0.14
9	0.09	0.12	0.11	0.10	0.07	0.05	0.05	0.03	0.06	0.08
10	0.11	0.09	0.08	0.08	0.06	0.03	0.02	0.03	0.03	0.03

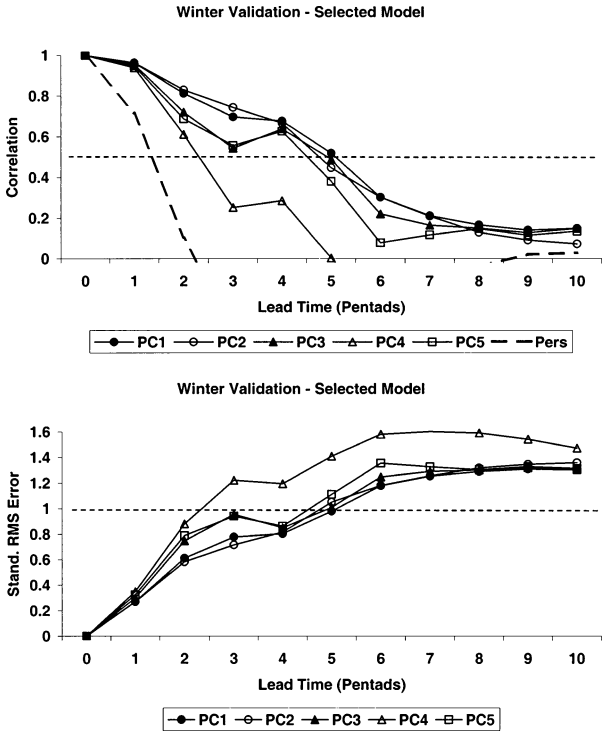

FIG. 5. Winter validation of selected forecast model. Each curve shows the validation of forecasts of PC1–PC5. (top) Correlations; (bottom) standardized rmse. Dashed line in the top panel is the forecast validation of PC1 obtained by persistence. Verification is performed on 11 winter seasons of independent data.

increasing the number of PCs as predictors [Eq. (6)]. As in the winter case, the increase in PCs as predictors is not as systematic as increasing the lags λ. At long lead times (i.e., three to six pentads), the results also suggest that increasing more than five PCs as predictors decrease the forecast skill.

The selected forecast models for the summer season assume the same form expressed in Eq. (7), that is, for each PC_K ($k = 1, 5$), the forecast models use a combination of the five most recent pentad values of the first five PCs of the combined EOF as predictors. The validations of the summer forecast models are shown in Fig. 7 and, in general, indicate useful forecast skills up to five pentads of lead time. It is interesting to note that PC4 shows higher skill relative to the winter case, whereas the opposite is observed for PC5.

Some final remarks regarding the construction of our winter and summer forecast models are worth mentioning. Our forecast models are based on the PCs derived from the combined EOF (OLR, U200, U850). We have reproduced the forecasts models described before, however using the PCs from EOF analysis of OLR only. Our selected forecast models [Eq. (7)] exhibit substantial gains in forecast skill relative to the models that use only the most recent pentads of PCs from the EOF of OLR only, which is equivalent to fixing $\lambda = 1$ pentad in Eq. (5). Such models have been investigated by Lo and Hendon (2000, see their Fig. 11). The gain in terms of correlations for PC1 (PC2) is about 28% (37%) averaged in winter and summer for one to four pentads of lead time. Increasing the lags, for instance, fixing $\lambda =$ 5 pentads in Eq. (5), as it is the case in our selected models, the gain in forecast skill is less significant. The gain for PC1 (PC2) is 2.2% (1.6%) averaged in winter and summer for one to four pentads of lead time. However, as indicated before, the models derived from the combined EOF (OLR, U200, U850) have the additional advantage of providing forecasts of all three fields together.

Our computation of combined EOF uses the entire year and the forecast models were then derived separating winter and summer seasons from the PCs. We have attempted to first separate the data into winter and summer seasons, compute the combined EOF, and then derive the forecast models. This second approach however introduces a subtle difficulty to the problem. Note

TABLE 4. Summer results from AR models fitted to the first five PCs of combined EOF analysis (OLR, U200, U850). Lag, m indicates the order of the AR model, R_m is the mth lag autocorrelation, $S_\epsilon^2(m)$ is the white noise residual variance, and BIC and AIC are the statistics used to evaluate the best order of the AR model (see text for details). Bold values indicate local minimum.

	Summer AR models				
	Lag, m	R_m	$S_\epsilon^2(m)$	BIC	AIC
PC1	**0**	1.00	1.101E-03	−3010.1	−3018.3
	1	0.68	5.951E-04	−3283.3	−3291.5
	2	0.07	2.639E-04	−3637.3	−3649.6
	3	−0.36	2.472E-04	−3659.1	−3675.5
	4	−0.46	2.282E-04	−3687.5	−3708.0
	5	−0.38	2.130E-04	**−3711.1**	**−3735.7**
	6	−0.26	2.128E-04	−3704.4	−3733.0
PC2	**0**	1.00	8.453E-04	−3127.5	−3135.6
	1	0.67	4.709E-04	−3387.2	−3395.4
	2	0.02	1.995E-04	−3761.4	−3773.7
	3	−0.39	1.749E-04	−3812.7	−3829.1
	4	−0.42	1.545E-04	−3860.7	−3881.2
	5	−0.30	1.447E-04	**−3882.6**	**−3907.2**
	6	−0.21	1.446E-04	−3876.0	−3904.7
PC3	**0**	1.00	1.025E-03	−3041.8	−3050.0
	1	0.65	5.922E-04	−3285.5	−3293.7
	2	0.00	2.650E-04	−3635.3	−3647.6
	3	−0.41	2.406E-04	−3671.2	−3687.6
	4	−0.43	2.154E-04	−3713.2	−3733.7
	5	−0.30	2.056E-04	**−3726.8**	**−3751.4**
	6	−0.18	2.054E-04	−3720.0	−3748.7
PC4	**0**	1.00	1.133E-03	−2997.6	−3005.8
	1	0.67	6.267E-04	−3260.3	−3268.5
	2	0.06	3.119E-04	−3563.0	−3575.3
	3	−0.30	2.640E-04	−3629.9	−3646.3
	4	−0.31	2.316E-04	−3681.1	−3701.6
	5	−0.27	2.034E-04	**−3731.4**	**−3756.0**
	6	−0.33	2.030E-04	−3725.3	−3753.9
PC5	**0**	1.00	1.088E-03	−3015.4	−3023.6
	1	0.56	7.429E-04	−3184.8	−3193.0
	2	−0.17	3.683E-04	−3489.2	−3501.5
	3	−0.44	3.176E-04	−3547.9	−3564.3
	4	−0.25	2.813E-04	−3594.7	−3615.2
	5	−0.10	2.588E-04	**−3624.6**	**−3649.2**
	6	−0.17	2.587E-04	−3617.6	−3646.3

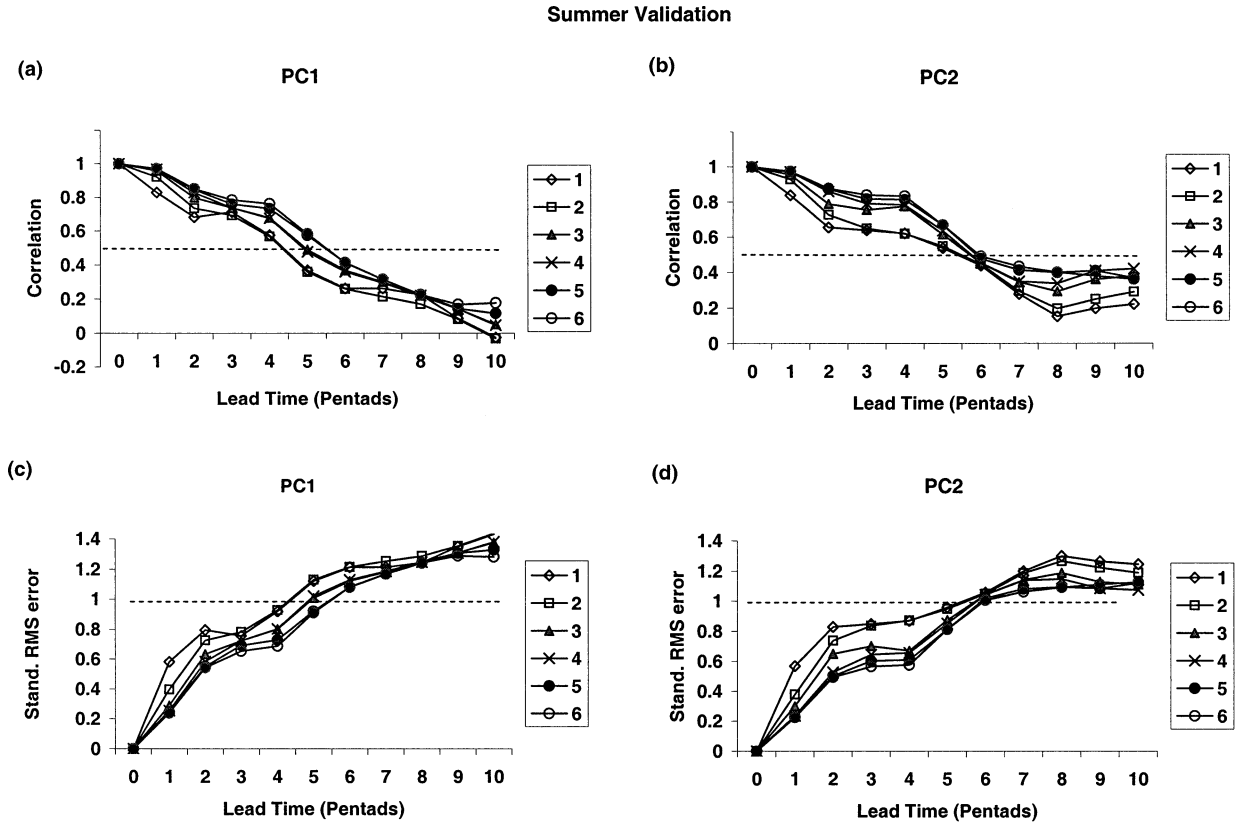

FIG. 6. Summer sensitivity test to increasing lags of PC predictors [see Eq. (5)]. (a), (b) Correlations between forecasts and validation values of PC1 and PC2. Each curve indicates the lag (one to six pentads). (c), (d) Standardized rmse between forecasts and validation values of PC1 and PC2. Verification is performed on 12 summer seasons of independent data.

TABLE 5. Summer forecast validations of (top) PC1 and (bottom) PC2. Lead times (pentads) are indicated in the leftmost vertical column. The number of PCs used as predictors are indicated in the first horizontal line (1–10) [see Eq. (7) and text for details]. Values indicate correlations between forecast and validation.

Summer validation—PC1 correlation										
Lead	1	2	3	4	5	6	7	8	9	10
1	0.68	0.83	0.82	0.83	0.82	0.81	0.82	0.83	0.84	0.84
2	0.02	0.68	0.67	0.67	0.67	0.65	0.66	0.67	0.69	0.69
3	0.46	0.71	0.71	0.71	0.71	0.71	0.71	0.71	0.71	0.71
4	0.55	0.58	0.57	0.59	0.60	0.58	0.58	0.58	0.58	0.55
5	0.37	0.37	0.34	0.37	0.37	0.31	0.30	0.29	0.29	0.26
6	0.15	0.26	0.24	0.19	0.23	0.21	0.14	0.14	0.15	0.15
7	−0.01	0.26	0.26	0.19	0.24	0.25	0.13	0.13	0.11	0.12
8	0.07	0.23	0.25	0.25	0.25	0.23	0.17	0.17	0.08	0.08
9	0.04	0.09	0.10	0.15	0.14	0.14	0.14	0.11	0.04	0.04
10	−0.01	−0.03	−0.05	0.03	−0.04	−0.05	−0.1691	−0.17	−0.15	0.15
Winter validation—PC2 correlation										
Lead	1	2	3	4	5	6	7	8	9	10
1	0.39	0.84	0.84	0.83	0.80	0.80	0.76	0.77	0.77	0.78
2	0.64	0.66	0.63	0.63	0.58	0.57	0.47	0.48	0.47	0.50
3	0.54	0.64	0.64	0.63	0.62	0.62	0.58	0.56	0.56	0.57
4	0.24	0.62	0.61	0.58	0.59	0.59	0.58	0.56	0.58	0.58
5	−0.05	0.54	0.52	0.50	0.50	0.51	0.49	0.49	0.50	0.50
6	0.21	0.44	0.45	0.46	0.46	0.45	0.43	0.43	0.43	0.42
7	0.23	0.28	0.32	0.38	0.33	0.33	0.33	0.27	0.27	0.26
8	0.19	0.15	0.18	0.12	−0.07	−0.07	−0.1619	−0.19	−0.15	0.15
9	0.13	0.20	0.20	−0.23	−0.28	−0.29	−0.2839	−0.28	−0.25	0.25
10	0.07	0.22	0.25	−0.09	−0.09	−0.06	−0.0489	−0.05	−0.03	0.04

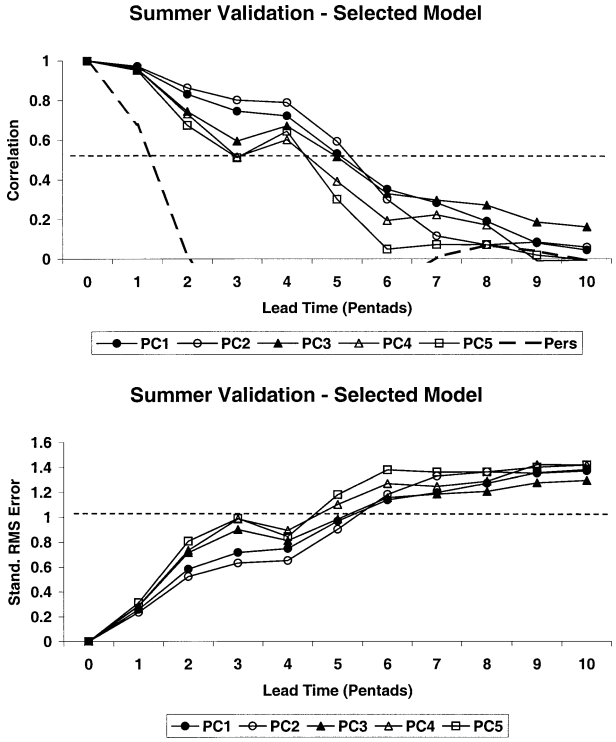

FIG. 7. Summer validation of selected forecast model. Each curve shows the validation of forecasts of PC1–PC5. (top) Correlations; (bottom) standardized rmse. Dashed line in the top panel is the forecast validation of PC1 obtained by persistence. Verification is performed on 12 summer seasons of independent data.

that our forecast models are based on previous values of the PCs ($\lambda = 5$). The separate computation of combined EOF in winter and summer seasons introduced discontinuities (or uncorrelated values) near the boundaries of winter and summer data, which significantly degraded the performance of the forecast models. The same comment applies if one attempts to use cross validation, instead of separating the data into developing and validation samples as used here. Nevertheless, as the forecast validation indicates, the methodology to derive our forecast models does capture the seasonal behavior of the MJO.

4. Statistical forecast skill

The final step in our statistical forecast system consists in reconstructing the fields of OLR, U200, and U850 using the forecasts of PC_K, ($k = 1, 5$) and the associated EOFs for lead times $\tau = 1, 10$ pentads. Namely,

$$Y(t + \tau) = \sum_{K=1}^{5} PC_K(t + \tau)EOF_K(Y), \qquad (8)$$

where Y is the forecast of the intraseasonal anomaly of OLR, U200, or U850 at lead time τ and $EOF_K(Y)$ is the kth EOF of OLR, U200, or U850.

In this section, we evaluate the spatial structure of the forecast skills. To accomplish this, the winter and summer forecast models were applied to the validation sample and correlations between forecasts and observed 20–90-day anomalies of OLR, U200, and U850 were computed.

The correlation between OLR forecasts verified against 20–90-day OLR anomalies during 11 extended winter seasons is shown in Fig. 8. A broad region of correlations greater than 0.5 at 5 days of lead time coincides with the region of largest intraseasonal variability in the Indian and western Pacific Oceans. Secondary correlation maxima are also found over tropical Africa and eastern South America and tropical Atlantic. The correlations decrease in magnitude for increased lead times, although they remain between 0.4 and 0.5 at 20 days of lead time over a large area in the Indian Ocean and western Pacific.

The winter forecast verification of U200 anomalies (Fig. 9) shows an extensive area of correlations greater than 0.4 at 5 days of lead time over the tropical belt. The maximum correlation in U200 forecasts is slightly to the north of the region of maximum OLR correlations. Note also that at 5 days of lead time, correlations are significantly high over the North Pacific indicating useful forecasts in the jet stream region. At 20 days of lead time, the U200 correlations are still above 0.5 over the Indian Ocean. Likewise, the correlation pattern found in the verification of U850 forecasts (Fig. 10), shows useful skill (above 0.5) at 5 days of lead time over the tropical region extending over nearly all longitudes but with a maximum over Indonesia. As in the U200 case, correlations are substantially high over a large region in the North Pacific. The correlations remain in the range of 0.4–0.5 at 20 days of lead time over Indonesia and the western Pacific Ocean.

The forecast verification of OLR anomalies against 20–90-day anomalies during the 12 summer seasons shows an extensive region of correlations above 0.5 over the eastern tropical hemisphere with two maxima over the Indian Ocean and western Pacific (Fig. 11). Another region of useful forecast skills is localized over the tropical eastern Pacific. As it was pointed out in the last section, we recall that our methodology computes combined EOFs using data from the entire year and then derives forecast models for winter and summer separately. Note however that the forecast verification does indicate that the methodology is capable of effectively capturing seasonal variations in OLR. Compare, for instance, the displaced skill toward the Indian–Asian monsoon as well as over Central America (cf. Fig. 8). For increasing lead times, the forecast skill decreases to 0.4–0.5 out to 20 days.

The correlations between U200 forecasts and 20–90-day anomalies during the summer season also display a pattern of high values over the Tropics (Fig. 12). In particular, regions with high correlations are observed over the Indian Ocean, Indonesia, and the eastern trop-

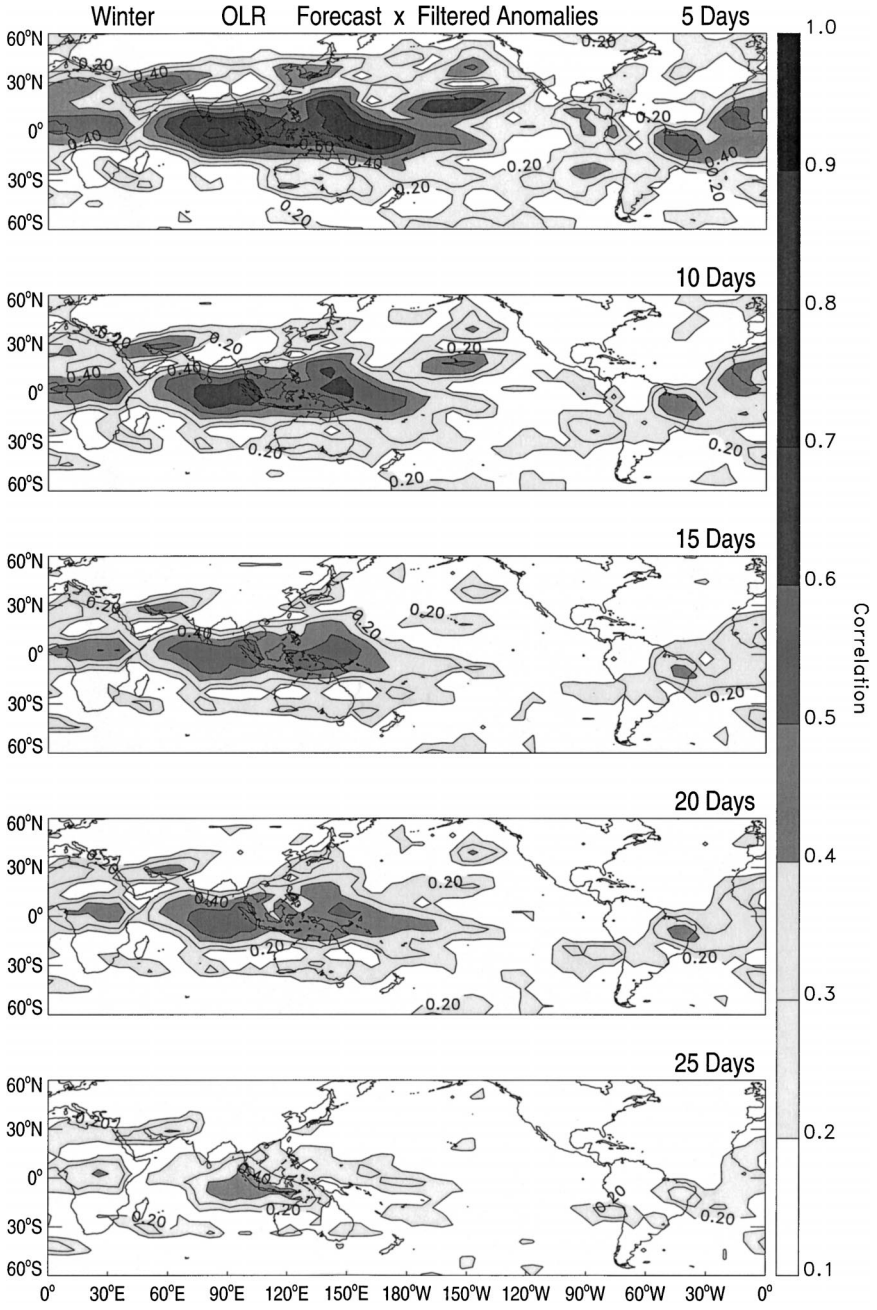

FIG. 8. Correlation between forecasts and validation values of 20–90-day anomalies of OLR. First contour is 0.2 and interval is 0.1. Lead times are indicated in each panel. Validation is performed on 11 winter seasons of independent data.

ical Pacific. Correlations of 0.4–0.5 at lead times of 20 days are still found in some tropical regions. The verification of U850 forecasts (Fig. 13) displays useful forecast skills over the entire Tropics at 5 days of lead time with two maxima over Indonesia and the eastern tropical Pacific. Correlations above 0.5 are still observed at 20 days of lead time.

The statistical forecast models used here have some similarity to the ones developed by Lo and Hendon (2000) in the sense that both models use linear regressions to predict future values of PCs. Although it is not our intent to compare both models, it is important to note at least three major differences. First, our methodology isolate intraseasonal variations by applying bandpass filtering in frequency domain, whereas Lo and Hendon (2000) remove the annual cycle, interannual variations (from regressions to sea surface temperature), and spatial filtering. It would be interesting to directly

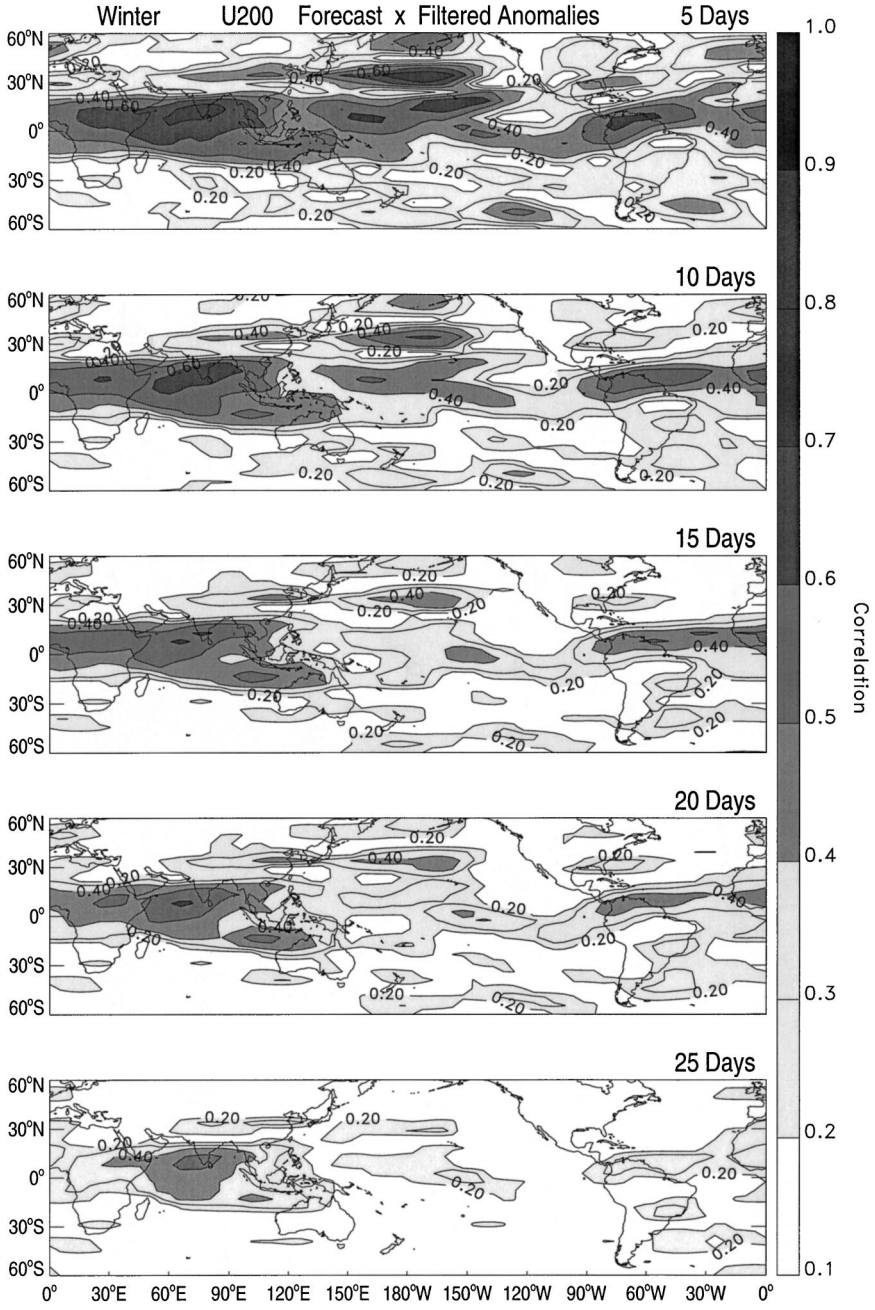

FIG. 9. Same as in Fig. 8, but for correlations between forecasts and validation values of 20–90-day anomalies of U200.

compare both filtering techniques. A difficult problem present in our methodology as well as in previous forecast models of intraseasonal variations is that, if applied in real-time forecasts, filtering likely incur in errors near the initial conditions due to edge effects in the time series. Second, the PCs in our model are derived from the combined EOF (OLR, U200, and U850). Third, our forecast models are based on multiple linear regression equations that include a larger number of predictors than in Lo and Hendon (2000). Although a direct comparison between both models is difficult to make, it appears that better forecast skills are obtained with the approach described here.

5. Summary and conclusions

Intraseasonal variations in tropical convective activity play a significant role in the coupled ocean–atmosphere system and the Madden–Julian oscillation is the primary mode of this variability. Recently, there has been an

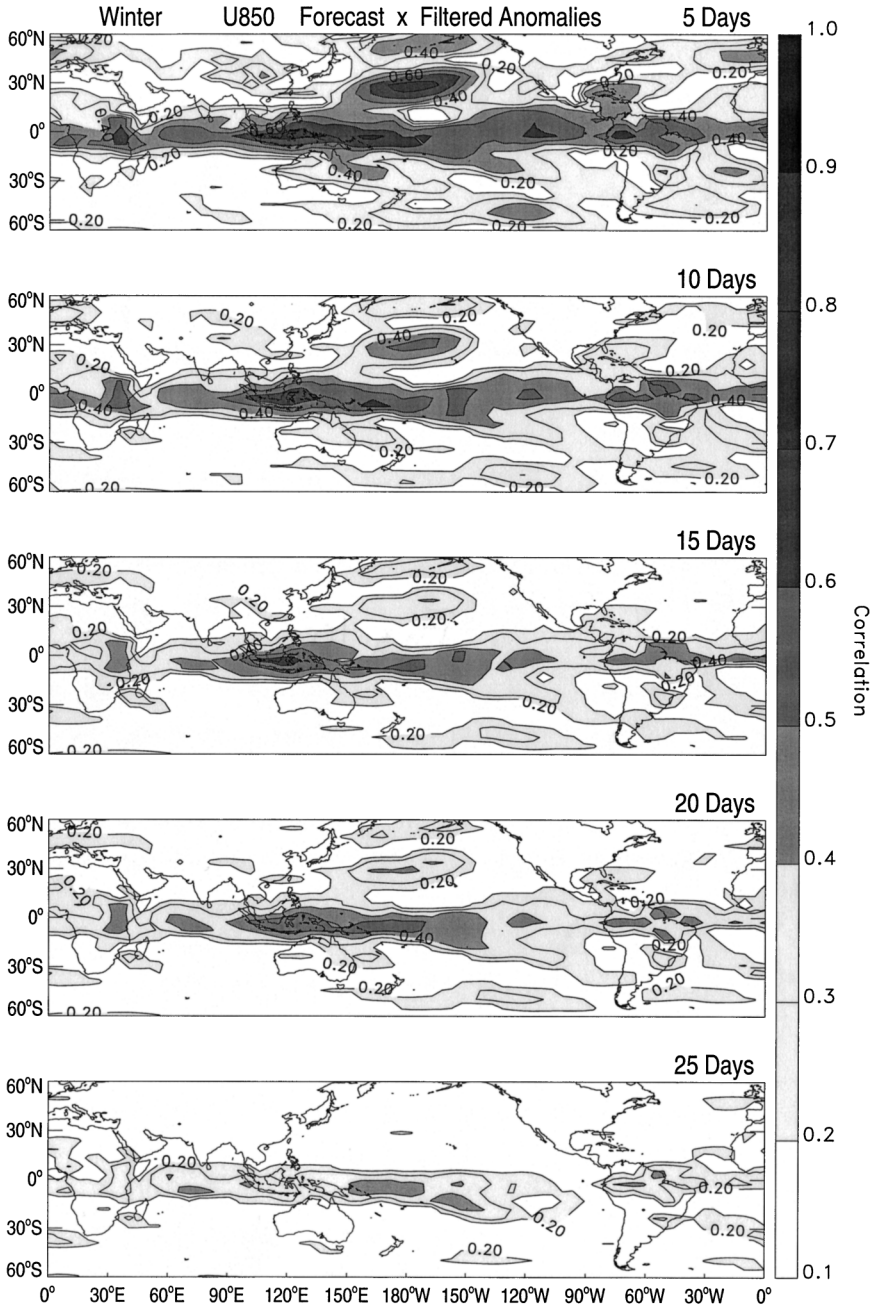

FIG. 10. Same as in Fig. 8, but for correlations between forecasts and validation values of 20–90-day anomalies of U850.

increasing interest in exploiting the predictability of weather and short-term climate variability on subseasonal time scales. This study describes statistical forecast models of intraseasonal variations. The models use the PCs of combined EOF analysis of 20–90-day anomalies of OLR, U200, and U850 data. Forecast models are developed for each lead time from 1 to 10 pentads and for winter and summer seasons separately. The forecast models use a combination of the five most recent pentad values of the first five PCs of the combined EOF (OLR, U200, U850) to predict the future values of a given PC_k ($k = 1, 5$). The spatial structures are obtained by reconstructing the fields of OLR, U200 and U850 using the forecasts of PC_k, ($k = 1, 5$) and the associated EOFs. Verification with independent winter and summer data indicates useful forecasts of the first five PCs extending up to five pentads of lead time. The verification against 20–90-day anomalies indicates useful forecasts of the reconstructed fields of OLR, U200, and U850 extending up to four pentads of lead time over most of

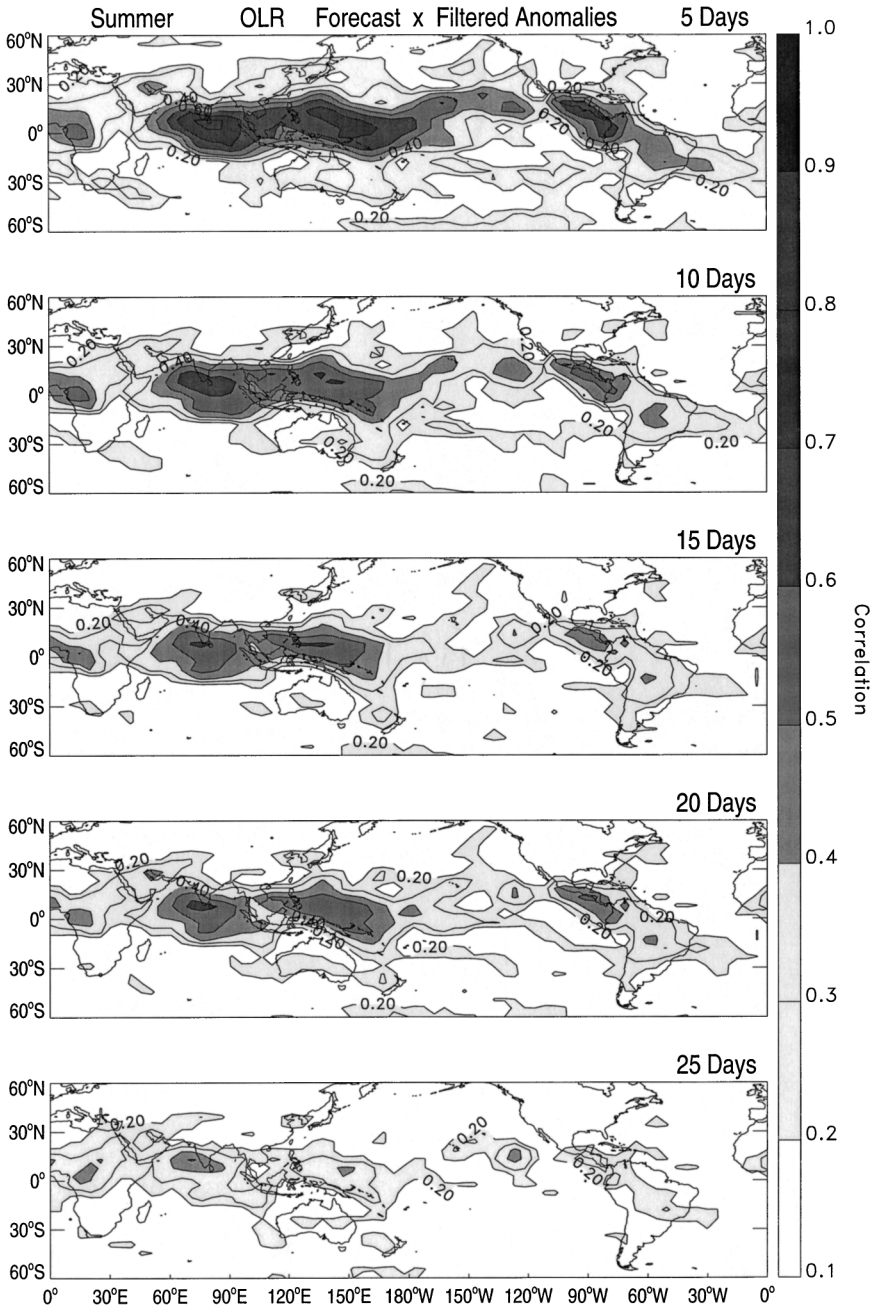

FIG. 11. Correlation between forecasts and validation values of 20–90-day anomalies of OLR. First contour is 0.2 and interval is 0.1. Lead times are indicated in each panel. Validation is performed on 12 summer seasons of independent data.

the Tropics. Furthermore, the statistical models provide useful forecasts of U200 and U850 intraseasonal anomalies up to two to three pentads of lead times in portions of the North Pacific region.

A fundamental question relates to the limit of theoretical predictability of the MJO. In a recent study, Waliser et al. (2003) addressed this topic with ensembles of ''twin'' predictability experiments with the National Aeronautics and Space Administration (NASA) Goddard Laboratory for Atmospheres (GLA) atmospheric general circulation model (AGCM) using specified annual cycle SSTs. A measure of potential predictability was constructed based on the ratio of the signal associated with the MJO and the mean square error between sets of twin forecasts. Analysis of the boreal winter predictability ratio indicates that useful predictability for this model's MJO extends out to about 25–30 days for velocity potential at 200 hPa and to about 10–15 days for rainfall.

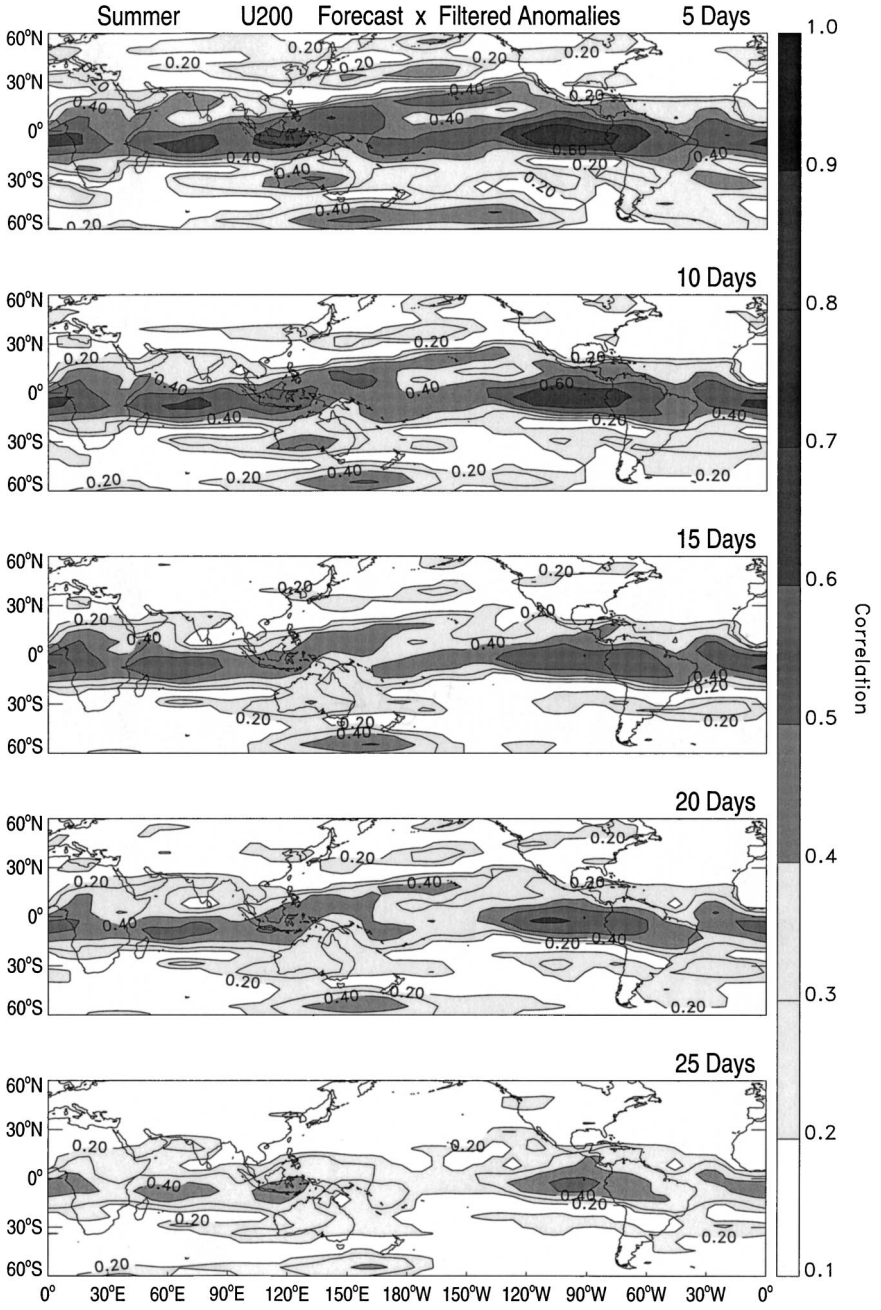

FIG. 12. Same as in Fig. 11, but for correlations between forecasts and validation values of 20–90-day anomalies of U200.

In addition, the predictability measure shows modest dependence on the phase of the MJO, with greater predictability for the convective phase at short ($<\sim$5 days) lead times and for the suppressed phase at longer ($>\sim$15 days) lead times. The predictability of intraseasonal variability during periods of weak MJO activity is significantly diminished compared to periods of strong MJO activity. A somewhat similar limit of predictability was found for the boreal summer season (Waliser et al. 2002b). However, a major characteristic of the MJO is its high degree of variability from case-to-case, seasonal, and interannual variations. Thus, estimating the dynamical predictability of the MJO for different characteristics (e.g., eastward propagations or interannual behavior) is a research area that needs to wait until realistic representations of the MJO in numerical forecast models are attained. Our current research focuses on using the statistical forecast models described here to monitor and predict the evolution of the MJO in real time (see online at www.icess.ucsb.edu/asr).

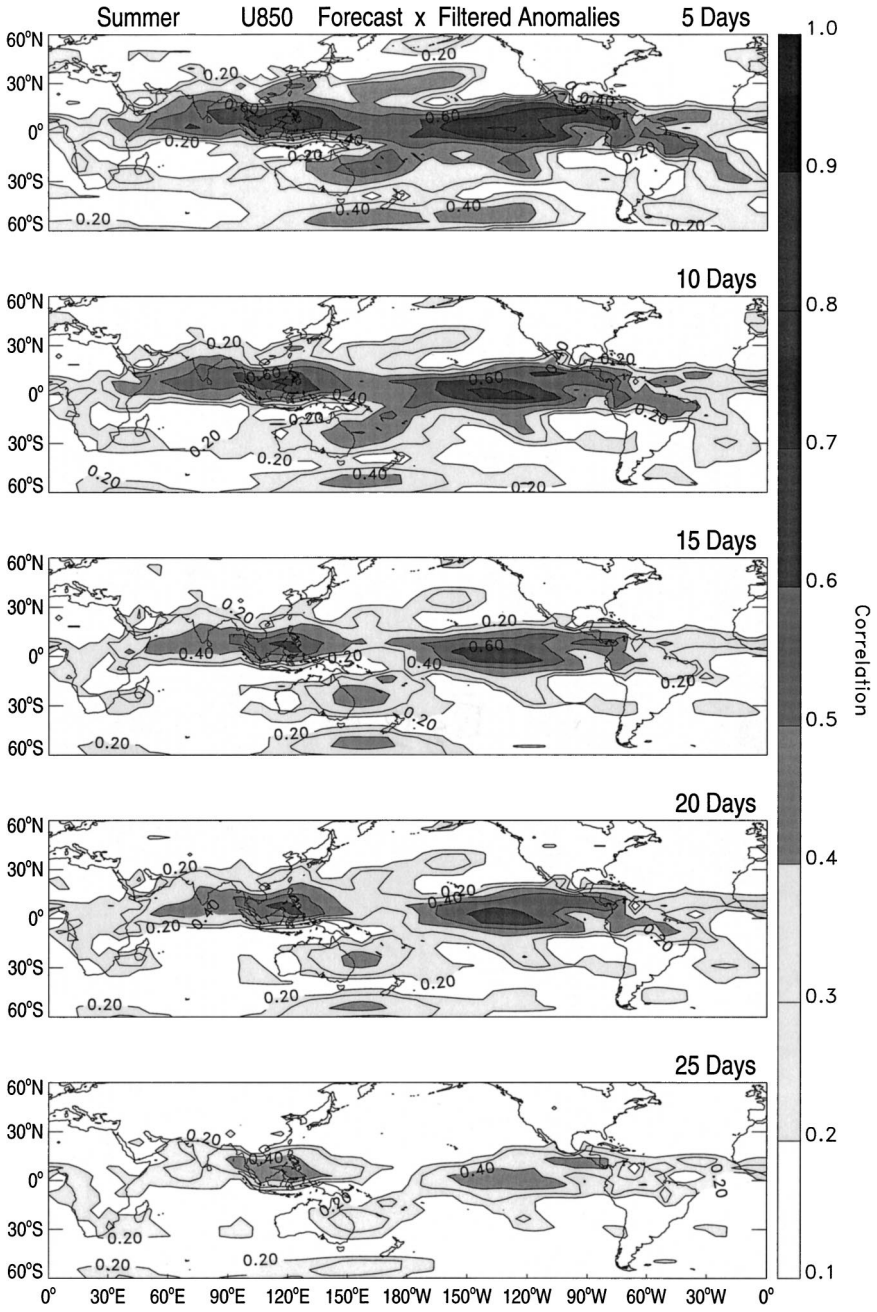

FIG. 13. Same as in Fig. 11, but for correlations between forecasts and validation values of 20–90-day anomalies of U850.

Acknowledgments. The authors would like to acknowledge the support of the National Center for Atmospheric Research (NCAR) and the Climate Prediction Center for making datasets available. NCAR is sponsored by the National Science Foundation. This study benefited from the following research grants: C. Jones—NOAA Office of Global Programs CLIVAR–Pacific Program (NA16GP1019), CLIVAR-PACS (NA16GP1020), and the National Science Foundation (ATM-0094387); D. E. Waliser—NOAA Office of Global Programs CLIVAR (NA16GP2021) and the National Science Foundation (ATM-0094416).

REFERENCES

Carvalho, L. M. V., C. Jones, and B. Liebmann, 2004: The South Atlantic convergence zone: Intensity, form, persistence, and relationships with intraseasonal to interannual activity and extreme rainfall. *J. Climate*, **17,** 88–108.

Chelliah, M., and P. Arkin, 1992: Large-scale interannual variability

of monthly outgoing longwave radiation anomalies over the global Tropics. *J. Climate,* **5,** 371–389.
Ferranti, L., T. N. Palmer, F. Molteni, and K. Klinker, 1990: Tropical–extratropical interaction associated with the 30–60-day oscillation and its impact on medium and extended range prediction. *J. Atmos. Sci.,* **47,** 2177–2199.
Hendon, H. H., B. Liebmann, M. Newman, J. D. Glick, and J. Schemm, 2000: Medium range forecast errors associated with active episodes of the Madden–Julian oscillation. *Mon. Wea. Rev.,* **128,** 69–86.
Higgins, R. W., and W. Shi, 2001: Intercomparison of the principal modes of interannual and intraseasonal variability of the North American monsoon system. *J. Climate,* **14,** 403–417.
——, J.-K. E. Schemm, W. Shi, and A. Leetmaa, 2000: Extreme precipitation events in the western United States related to tropical forcing. *J. Climate,* **13,** 793–820.
Hirose, M., and J. E. Kutzbach, 1969: An alternate method for eigenvector computations. *J. Appl. Meteor.,* **8,** 701.
Jenkins, G. M., and D. G. Watts, 1968: *Spectral Analysis and Its Applications.* Holden-Day, 523 pp.
Jones, C., 2000: Occurrence of extreme precipitation events in California and relationships with the Madden–Julian oscillation. *J. Climate,* **13,** 3576–3587.
——, and J.-K. E. Schemm, 2000: The influence of intraseasonal variations on medium-range weather forecasts over South America. *Mon. Wea. Rev.,* **128,** 486–494.
——, and L. M. V. Carvalho, 2002: Active and break phases in the South American Monsoon System. *J. Climate,* **15,** 905–914.
——, D. E. Waliser, and C. Gautier, 1998: The influence of the Madden–Julian oscillation on ocean surface heat fluxes and sea surface temperature. *J. Climate,* **11,** 1057–1072.
——, ——, J. K. Schemm, and W. K. Lau, 2000: Prediction skill of the Madden–Julian oscillation in dynamical extended range forecasts. *Climate Dyn.,* **16,** 273–289.
——, M. V. Carvalho, R. W. Higgins, D. E. Waliser, and J.-K. Schemm, 2004a: Climatology of tropical intraseasonal convective anomalies: 1979–2002. *J. Climate,* **17,** 523–539.
——, D. E. Waliser, W. K. Lau, and W. Stern, 2004b: The Madden–Julian oscillation and its impact on Northern Hemisphere weather predictability. *Mon. Wea. Rev.,* **132,** 1462–1471.
Kalnay, E., and Coauthors, 1996: The NCEP/NCAR 40-Year Reanalysis Project. *Bull. Amer. Meteor. Soc.,* **77,** 437–471.
Katz, R. W., 1982: Statistical evaluation of climate experiments with general circulation models: A parametric time series modeling approach. *J. Atmos. Sci.,* **39,** 1446–1455.
Kessler, W. S., 2001: EOF representations of the Madden–Julian oscillation and its connection with ENSO. *J. Climate,* **14,** 3055–3061.
Kutzbach, J. E., 1967: Empirical eigenvectors of sea-level pressure, surface temperature and precipitation complexes over North America. *J. Appl. Meteor.,* **6,** 791–802.
Lau, K. M., and P. H. Chan, 1986: Aspects of the 40–50-day oscillation during the northern summer as inferred from outgoing longwave radiation. *Mon. Wea. Rev.,* **114,** 1354–1367.
——, and F. C. Chang, 1992: Tropical intraseasonal oscillation and its prediction by the NMC operational model. *J. Climate,* **5,** 1365–1378.
Lo, F., and H. H. Hendon, 2000: Empirical prediction of the Madden–Julian oscillation. *Mon. Wea. Rev.,* **128,** 2528–2543.
Lucas, L. E., D. E. Waliser, P. Xie, J. E. Janowiak, and B. Liebmann, 2001: Estimating the satellite equatorial crossing time biases in the daily, global outgoing longwave radiation data set. *J. Climate,* **14,** 2583–2605.
Madden, R. A., and P. R. Julian, 1994: Observations of the 40–50-day tropical oscillation—A review. *Mon. Wea. Rev.,* **122,** 814–837.
McPhaden, J. M., 2002: Mixed layer temperature balance on intraseasonal timescales in the equatorial Pacific Ocean. *J. Climate,* **15,** 2632–2647.
Mo, K. C., 2000: Intraseasonal modulation of summer precipitation over North America. *Mon. Wea. Rev.,* **128,** 1490–1505.
——, 2001: Adaptive filtering and prediction of intraseasonal oscillations. *Mon. Wea. Rev.,* **129,** 802–817.
Nogués-Paegle, J., L. A. Byerle, and K. C. Mo, 2000: Intraseasonal modulation of South American summer precipitation. *Mon. Wea. Rev.,* **128,** 837–850.
North, G. R., T. L. Bell, and R. F. Cahalan, 1982: Sampling errors in estimation of empirical orthogonal functions. *Mon. Wea. Rev.,* **110,** 699–706.
Preisendorfer, R. W., 1988: *Principal Component Analysis in Meteorology and Oceanography.* Developments in Atmospheric Science, Vol. 17, Elsevier, 425 pp.
Rasmusson, E. M., and P. A. Arkin, 1993: A global view of large-scale precipitation variability. *J. Climate,* **6,** 1495–1522.
Salby, M. L., and H. H. Hendon, 1994: Intraseasonal behavior of clouds, temperature, and motion in the Tropics. *J. Atmos. Sci.,* **51,** 2207–2224.
Schubert, S., R. Dole, H. van den Dool, M. Suarez, and D. Waliser, 2002: *Proceedings Prospects for Improved Forecasts of Weather and Short-Term Climate Variability on Subseasonal (2 Week to 2 Month) Time Scales.* Vol. 23, Mitchellville, MD, NASA, NASA/TM 2002-104606, 171 pp.
Waliser, D. E., C. Jones, J. K. Schemm, and N. E. Graham, 1999: A statistical extended-range tropical forecast model based on the slow evolution of the Madden–Julian oscillation. *J. Climate,* **12,** 1918–1939.
——, W. Stern, S. Schubert, and K. M. Lau, 2002: Dynamic predictability of intraseasonal variability associated with the Asian summer monsoon. *Quart. J. Roy. Meteor. Soc.,* **129,** 2897–2925.
——, K. M. Lau, W. Stern, and C. Jones, 2003: Potential predictability of the Madden–Julian oscillation. *Bull. Amer. Meteor. Soc.,* **84,** 33–50.
Wheeler, M., and K. Weickmann, 2001: Real-time monitoring and prediction of modes of coherent synoptic to intraseasonal tropical variability. *Mon. Wea. Rev.,* **129,** 2677–2694.
Whitaker, J. S., and K. M. Weickmann, 2001: Subseasonal variations of tropical convection and week-2 prediction of wintertime western North American rainfall. *J. Climate,* **14,** 3279–3288.
Wilks, D. S., 1995: *Statistical Methods in the Atmospheric Sciences.* Academic Press, 467 pp.
Yasunari, T., 1979: Cloudiness fluctuations associated with the Northern Hemisphere monsoon. *J. Meteor. Soc. Japan,* **57,** 227–242.